Tellus (2003), 55B, 914–934
Printed in UK. All rights reserved

TELLUS
ISSN 0280–6509

Regional climate effects of aerosols over China: modeling and observation

By YUN QIAN[1]*, L. RUBY LEUNG[1], STEVEN J. GHAN[1] and FILIPPO GIORGI[2], [1]*Pacific Northwest National Laboratory, P.O. Box 999, Richland, Washington 99352, USA;* [2]*Abdus Salam International Center for Theoretical Physics, Trieste, Italy*

(Manuscript received 8 November 2002; in final form 17 February 2003)

ABSTRACT

We present regional simulations of aerosol properties, direct radiative forcing and aerosol climatic effects over China, and compare the simulations with observed aerosol characteristics and climatic data over the region. The climate simulations are performed with a regional climate model, which is shown to capture the spatial distribution and seasonal pattern of temperature and precipitation. Aerosol concentrations are obtained from a global tracer-transport model and are provided to the regional model for the calculation of radiative forcing. Different aerosols are included: sulfate, organic carbon, black carbon, mineral dust, and sea salt and MSA particles. Generally, the aerosol optical depth is well simulated in both magnitude and spatial distribution. The direct radiative forcing of the aerosol is in the range –1 to –14 W m^{-2} in autumn and summer and -1 to –9 W m^{-2} in spring and winter, with substantial spatial variability at the regional scale. A strong maximum in aerosol optical depth and negative radiative forcing is found over the Sichuan Basin. The negative radiative forcing of aerosol induces a surface cooling in the range –0.6 to –1.2 °C in autumn and winter, –0.3 to –0.6 °C in spring and 0.0 to –0.9 °C in summer throughout East China. The aerosol-induced cooling is mainly due to a decrease in daytime maximum temperature. The cooling is maximum and is statistically significant over the Sichuan Basin. The effect of aerosol on precipitation is not evident in our simulations. The temporal and spatial patterns of the temperature trends observed in the second half of the twentieth century, including different trends for daily maximum and minimum temperature, are at least qualitatively consistent with the simulated aerosol-induced cooling over the Sichuan Basin and East China. This result supports the hypothesis that the observed temperature trends during the latter decades of the twentieth century, especially the cooling trends over the Sichuan Basin and some parts of East China, are at least partly related to the cooling induced by increasing atmospheric aerosol loadings over the region.

1. Introduction

Atmospheric aerosols can influence climate directly by scattering and absorbing solar radiation and indirectly by modifying the microphysical and optical properties of clouds. Human activities represent an important source of airborne particulate material (IPCC, 2001), and indeed some studies have found substantial radiative forcing on the climate system by aerosols of anthropogenic origin (Rodhe, 1999; Penner, 2001; Ramaswarmy, 2001). A number of global models have calculated the direct and indirect radiative forcing of aerosols, mostly of anthropogenic origin (e.g. sulfate and soot), based on aerosol concentrations simulated with global chemical transport models coupled with General Circulation Models (GCMs) or driven by observed reanalysis data (e.g. Haywood and Ramaswamy, 1998; Barrie et al., 2001; Ghan et al., 2001a,b).

A region where the effects of anthropogenic aerosols are especially important is East Asia, one

*Corresponding author.
e-mail: yun.qian@pnl.gov

of the most populated and rapidly developing regions during the last decades. The ever-growing human activities have led to a rapid and continued increase in the emission of aerosol precursors (Wei, 1995; Ren et al., 1997). A number of studies (e.g. Hayami and Ichikawa, 1995; Phadnis et al., 1998; Qian et al., 2001) have simulated the transport and distribution of aerosols over East Asia based on trajectory analysis or three dimensional tracer models.

In particular, a series of recent studies investigated the role of anthropogenic aerosols in modifying the climate of East Asia with the use of a coupled regional climate/chemistry aerosol model. The modeling system was developed by Qian and Giorgi (1999) and Qian et al. (2001) by coupling a regional climate model (RegCM; Giorgi et al., 1993a,b) and a simplified version of a sulfur chemistry model based on a full chemistry-transport model (RADM; Chameides et al., 1999; Luo et al., 2000a). The coupled modeling system incorporated radiatively active aerosols, such as sulfate and soot. Using this model, Giorgi et al. (2002; 2003) (hereafter referred to as G0203) completed a series of regional simulations aimed at investigating the direct and indirect radiative forcing and climatic impacts of anthropogenic sulfate and fossil fuel soot over East Asia. They found that the direct effects of anthropogenic sulfate produces a surface cooling of -0.1 to $-0.7\,^{\circ}$C, which is maximum over the Sichuan Basin of southwest China and it is statistically significant over various areas of China. When both direct and indirect effects were included the surface cooling was enhanced, it locally exceeded $-1\,^{\circ}$C and it was statistically significant over more extended regions of China. The direct forcing was dominant in the cold season, while the indirect effect forcing was dominant in the summer monsoon season, when precipitation and cloudiness are maximum over East China. These results were generally consistent with the observed temperature record over East China during the last decades (Qian and Giorgi, 2000).

The primary shortcoming of the G0203 studies was that their model only included anthropogenic sulfate and fossil-fuel soot. The mass concentration of fossil-fuel soot was crudely estimated by assuming a linear relationship between soot and sulfate concentration. The assumption of external aerosol mixing was used in their model. In reality, however, soot (or black carbon, BC), originates not only from fossil-fuel consumption, but also from biomass burning (Penner, 2001). Furthermore, other aerosols, such as organic carbon (OC), mineral dust (Liousse et al., 1996; He et al., 2001) over land and sea salt and methane sulfonic acid (MSA) over ocean, are abundant over East Asia. Chameides et al. (1999) and G0203 crudely assessed the effects of these other aerosols by doubling the sulfate concentration or optical depth in a series of sensitivity experiments. However, different aerosols may have different spatial and temporal distributions. Furthermore, carbonaceous aerosols have optical properties different from sulfate. While sulfate and OC mostly reflect solar radiation back to space, BC is a good absorber of solar radiation, and thus induces heating of the lower troposphere. Therefore, they have different effects on the vertical structure of the atmosphere and possibly on the hydrologic cycle of the region (Ramanathan et al., 2001; Menon et al., 2002). It is thus evident that a simple doubling of the sulfate concentration cannot properly reproduce the effects of other types of aerosols.

To understand the climatic effects of aerosols over East Asia, a number of studies have attempted to identify the climate signal associated with increasing aerosol amounts using observed climate and aerosol concentration records for the last decades. Li et al. (1995) conducted a limited analysis of the temperature record over the Sichuan province and speculated that the cooling effects due to the aerosol might be responsible for the observed decrease in temperature over the area. Xu (2001) analyzed radiation and climate data and argued that changes in the mid-summer rain belt in central East China may be related to increasing SO_2 emissions in China. Based on an analysis of temporal and spatial patterns of pollutant emissions, observed aerosol extinction coefficient, sunshine duration and surface air temperature records for the past 45 years, Qian et al. (1996), Qian and Giorgi (2000) and Kaiser and Qian (2002) hypothesized that the observed cooling trends are at least partially related to the increase of anthropogenic aerosols over China.

All these modeling and observational studies clearly show that atmospheric aerosols of anthropogenic and natural origin have likely affected the climate of East Asia in a significant way and will likely continue to do so in the future. They also show the difficulty of studying this issue due to the varied nature and characteristics of the aerosol involved and the limitations of present modeling tools and observation records.

This work extends previous studies by combining more comprehensive modeling and observational tools to improve our understanding of the effects of aerosol on climate conditions in China. On the modeling side, we include the radiative effects of six types of primary

natural and anthropogenic aerosols within the framework of a regional climate model. Unlike G0203, the aerosol concentrations are not calculated within the regional model but are produced by off-line simulations with a global chemistry-aerosol model. Giorgi et al. (2002) showed that local aerosol/climate feedbacks play only a secondary role in determining the aerosol concentrations, so that an off-line approach is suitable to address this problem.

By incorporating a larger set of natural and anthropogenic aerosols, our simulations can be more realistically compared to the observed climatic record. In this paper we utilize a range of more comprehensive observed datasets and analysis tools to determine the effect of increasing aerosols in the historical temperature record over the region. At present, our model only includes the direct aerosol effects. Giorgi et al. (2003) clearly show that indirect effects can be important in affecting the surface climate signal, particularly in the warm season, and we plan to address this issue in future work.

2. Model and simulation strategy

2.1. Regional climate model description

The regional climate model used in this study is based on Version 3 of the Penn State/NCAR Mesoscale Model MM5 (Grell et al., 1993). Leung et al. (2003a) describe the modifications made to MM5 for regional climate application. A 20-yr regional climate simulation driven by the NCEP/NCAR reanalyses for the western U.S. was found to compare very well with observations (Leung et al., 2003a,b). After performing several short sensitivity runs to guide the selection of physics parameterizations, the following schemes were selected for our experiments over East Asia: the improved CCM2 radiative transfer scheme (Briegleb, 1992; Ghan et al., 2001b), the Grell cumulus convection parameterization (Grell et al., 1993), the Reisner mixed-phase cloud microphysics scheme (Reisner et al., 1998), the counter-gradient boundary layer scheme (Hong and Pan, 1996; Troen and Mahrt, 1986), and the Oregon State University Land Surface Model (Chen et al., 1996).

2.2. Aerosol parameterization

Aerosols in the model are represented by a set of modes characterized by log-normal particle size distributions. The size distribution of each mode is determined by the number concentration, the mass of each component, and the width of the distribution. Four aerosol modes are currently treated: Aiken, accumulation, coarse sea-salt and coarse soil dust. Table 1 lists the chemical components and geometric properties of each mode. The optical properties of each chemical component are listed in Table 2. While internal mixing of chemical components is assumed within each mode, the modes themselves are externally mixed. In general, the primary particles are externally mixed near their sources, but aged aerosols become more internally mixed.

Table 1. *Table Aerosol mode chemical components, geometric standard deviation (σ_g), and nominal geometric mean diameter size distribution,* D_{gN}

Mode	Chemical components	σ_g	D_{gN} (μm)
Aitken	Sulfate, MSA, OC, BC	1.6	0.026
Accumulation	Sulfate, MSA, OC, BC, sea-salt, soil dust	1.8	0.11
Coarse sea-salt	Sea-salt, sulfate, MSA	2.0	2.0
Coarse soil dust	Soil dust, sulfate	1.8	1.0

One of the most important factors contributing to the radiative properties of aerosol is water uptake. We use the Kohler theory to represent the hygroscopic growth (Ghan et al., 2001b). For each aerosol mode we express water uptake in terms of relative humidity, the surface mean dry radius, the relative contributions of each component of the aerosol to the total particle hygroscopicity, and the water on the aerosol from the previous time step.

We estimate the radiative forcing of aerosols by calculating the net downward radiative flux at the top of the atmosphere (F) twice in a simulation, once with aerosol scattering and absorption included (F_{aer}), and once with aerosol effects neglected (F_{noaer}). The direct forcing of aerosols (F_{direct}) can then be determined from the difference between F_{aer} and F_{noaer}. As mentioned, the indirect radiative effects of aerosols are not included in this study.

2.3. Experiment design

The model domain encompasses most of China and adjacent ocean areas. It is centered at 32.0°N and 107.5°E, with a horizontal grid spacing of 60 km (Fig. 1). The model includes 23 vertical levels extending up to 100 mbar. The period of simulation

Table 2. *For each aerosol chemical component, ν (the number of ions into which the salt disassociates), ϕ (the osmotic coefficient), ε (the soluble mass fraction), ρ (the material density),* M *(the molecular weight of the aerosol material),* B *(the hygroscopicity) and the refractive index for solar and infrared wavelengths*

Component	ν	ϕ	ε	ρ	M	B	Refractive index	
							Solar	Infrared
Water				1.00	18		1.33+0.0i	1.18+0.68i
Ammonium sulfate	3	0.7	1.0	1.77	132	0.51	1.53+0.0i	1.98+0.06i
MSA	3	0.7	1.0	1.48	96	0.58	1.53+0.0i	1.98+0.06i
Sea salt	2	1.0	1.0	1.90	59	1.16	1.50+0.0i	1.50+0.01i
Soil dust	–	–	0.13	2.60	–	0.14	1.50+0.002i	1.62+0.12i
Organic carbon	–	–	–	1.00	–	0.14	1.55+0.0i	1.70+0.07i
Black carbon	–	–	–	1.7	–	5×10^{-7}	1.90+0.60i	2.22+0.73i

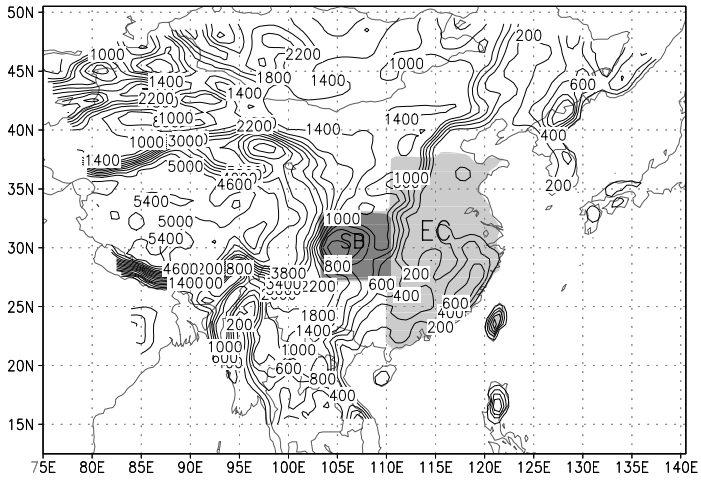

Fig. 1. Regional model domain and topography used in the regional simulations. Units are m, with contour interval of 200 m. Also shown are two regions for subcontinental scale analysis: SB, Sichuan Basin; EC, East China.

is from 1 April 1994 to 31 May 1999. The first two months of simulations are not used in the analysis to allow for spin-up of the model. Large-scale meteorological and surface data (e.g. sea surface temperature) from the European Center for Medium-Range Weather Forecast Tropical Ocean Global Atmospheres (ECMWF-TOGA) analyses are used to construct the initial and boundary conditions for the regional model. These boundary conditions include 12-hourly large-scale temperature, atmospheric moisture, winds, geopotential height, surface pressure and sea surface temperature, all spatially interpolated horizontally and vertically from the analyses grids and pressure levels to that of MM5.

The climatic effects of aerosols, both natural and anthropogenic, are assessed by comparing two experiments for the full 5-yr simulation periods. In the first, or control experiment (CON), the aerosol concentration is set to zero in the radiation calculations. In the second, or aerosol direct effect experiment (DIR), monthly averaged mass and number concentrations of six types of dry aerosol particles are prescribed in the radiation calculations based on a 1-yr simulation performed with the global chemical transport model MIRAGE (Model for Integrated Research on Atmospheric Global Emissions).

MIRAGE is composed of two fully coupled atmospheric models: the Pacific Northwest National Laboratory (PNNL) Global Chemistry Model (GChM, Luecken et al., 1991; Benkovitz et al., 1994) and the PNNL version of the National Center for Atmospheric Research (NCAR) Community Climate Model

(CCM2) (Hack et al., 1993). GChM incorporates emissions of trace gases and primary aerosols from anthropogenic and natural sources and simulates processes of transport, gas-phase and aqueous-phase conversion, condensation, nucleation and coagulation, dry deposition and wet removal. When running in coupled mode, the CCM2 uses the aerosol fields from GChM in the computation of radiative scattering and absorption, and cloud droplet nucleation. GChM in turn uses transport and cloud/precipitation fields from the CCM2 in the computation of the aerosol fields. The winds, temperature and surface pressure used by GChM are nudged to the ECMWF reanalysis data. In this study, MIRAGE is only run for one year, from June 1994 to May 1995 at T42 (approximately $2.8^\circ \times 2.8^\circ$) resolution.

Because of the strong dependence of hygroscopic growth on relative humidity (RH), for RH above 90% even very small biases in the simulated RH can seriously affect the hygroscopic growth of aerosols. Ghan et al. (2001b) found that the simulated RH by MIRAGE exceeds 99% much more often than the ECMWF-analyzed RH, so they prescribed relative humidity based on ECMWF reanalysis in MIRAGE when calculating the hygroscopic effects of aerosols. In this study, relative humidity calculated directly by MM5 is used to calculate the hygroscopic growth.

2.4. Datasets

Through a bilateral agreement between the U.S. Department of Energy and the China Meteorological Administration on joint research on "Global and regional climate change" (Riches et al., 2000), aerosol and climate datasets for China have been made available to enable the investigation of the role of anthropogenic aerosols in climate change. Two sets of observed climatic data, including daily maximum and minimum surface temperature and daily mean temperature and precipitation, have been used to analyze the climate conditions of China. The first dataset, developed by the National Climatic Data Center (NCDC), includes data from over 600 stations in China for 1994–1999 and is used to validate the simulated regional climate.

The second dataset, developed by the Climate Research Unit (CRU) of the East Anglia University (New et al., 2000), consists of monthly-averaged global surface air temperature and precipitation data covering the period 1954–1998 at 0.5 degree spatial resolution. This is used to evaluate the long-term trends of temperature and precipitation. New et al. (2000) provides estimates of uncertainty associated with this climatological data.

Aerosol optical data used in this study include the aerosol optical depth (AOD) and the surface aerosol extinction coefficient (AEC). The AOD data, described by Luo et al. (2000b; 2001), are multiple-year averages for 45 stations in China. The AEC data, which includes monthly averages for the full 5-yr simulation period over 625 stations in China, are retrieved from the visual range data using the method described by Middleton (1954).

3. Control simulation

3.1. Climate simulation

In this section we discuss the results of the control run to evaluate the model basic climatology. Figure 2 shows the 5-yr mean warm season (June–July–August) and cold season (December–January–February) temperature in the simulation and observations. The simulated surface air temperature patterns generally agree well with the observations throughout most of China. In JJA, the simulated temperature is close to the observed over northern China. The temperature patterns over Northeast China, Inner Mongolia, and the Xinjiang area are well captured. The simulation is, however, 2–3 °C cooler than observed in southern China and parts of central China. In DJF, the strong latitudinal temperature gradient is well simulated, but the model exhibits a cold bias of -2 to -3 °C over most areas of China.

We also compared the simulated daily maximum ($T_{\max}$) and daily minimum ($T_{\min}$) temperature with observations (not shown). In JJA, similar to the mean temperature, both $T_{\max}$ and $T_{\min}$ simulated by the model are 2–3 °C colder than observed. In DJF, the simulated $T_{\max}$ is close to observations except for a warm bias of 1–2 °C over central China. However, the simulated $T_{\min}$ is 3–6 °C colder than observed over most areas of China. It is thus clear that in DJF the cold bias of the simulated mean surface air temperature is mainly due to the bias of $T_{\min}$.

Figure 3 shows the simulated and observed precipitation in JJA and DJF. Precipitation over China is low in winter and high in summer in association with the East Asia monsoon. The model captures this seasonal pattern very well. More specifically, precipitation is generally well simulated by the model in summer,

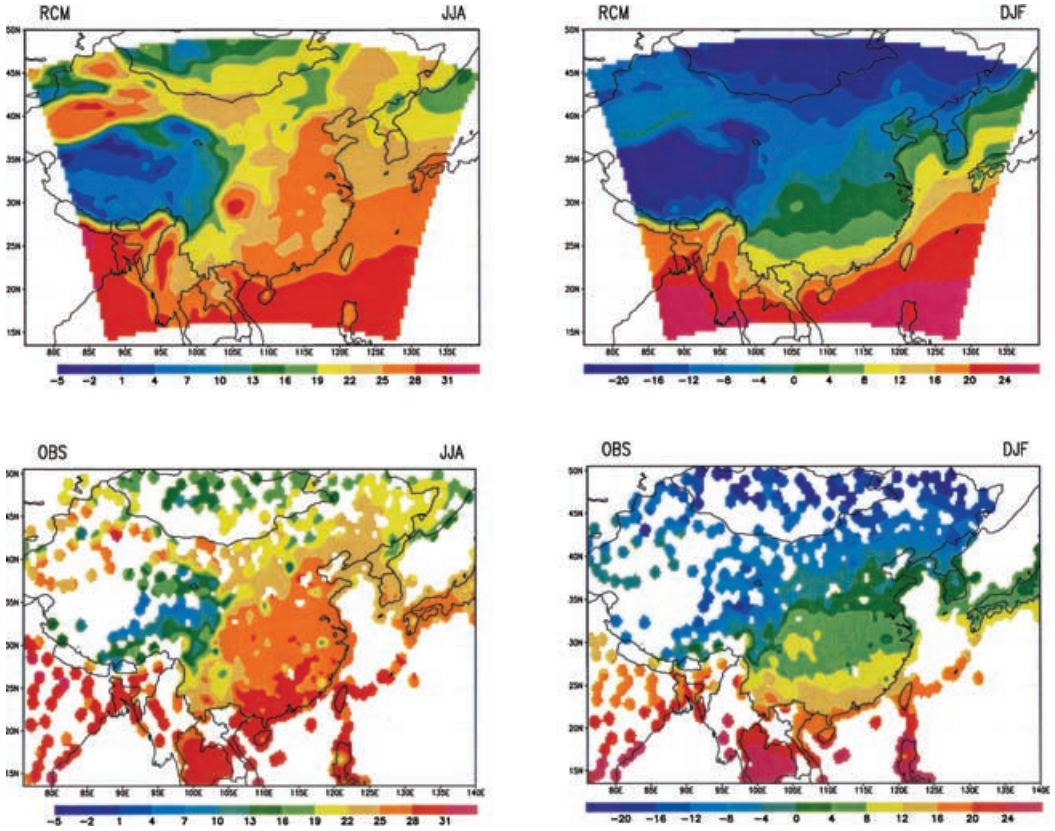

Fig. 2. Simulated (CON experiment) and observed seasonal mean surface air temperature during warm (June–July–August, JJA) and cold (December–January–February, DJF) seasons. Shading interval is 3 °C for JJA and 4 °C for DJF.

except for an underprediction of the maximum rainfall over the lower reaches of the Yangtze River, South Korea and southern Japan. The simulated Meiyu rainband associated with the East Asian summer monsoon shows a realistic narrow banded structure with a northeast–southwest orientation, heavy precipitation centers near the southwest corner of the rainband, and intense precipitation in the southern China coastal regions and Taiwan. However, the rainband lacks the intensity found in the observations. During winter, the differences between simulated and observed precipitation are relatively minor.

3.2. *Aerosol simulation*

3.2.1. Aerosol composition. Figure 4 shows the spatial distributions of the annual mean column mass in the four modes for sulfate, OC, BC, dust, sea salt, MSA, water in aerosol and their total sum. As mentioned, the aerosol concentration is simulated by the MIRAGE model and used as input to the MM5. The sulfate burden exhibits a minimum over west China and Tibet and a maximum over the Sichuan Basin and the area encompassing the Huabei region in northeast china, the Yellow Sea and Korea. This distribution is consistent with that obtained in the regional model simulations of Qian et al. (2001) and G0203 and the global model simulations by Penner (2001) and Barrie et al. (2001). The burden of BC and OC is maximum over the Huabei region, and the spatial distribution patterns of the two carbon aerosol types is similar. The mass of soil dust is primarily located over north and northwest China and is maximum in spring (March–June), the season of maximum occurrence of dust storms over northern and/or northwest China (Qian et al., 1999). Sea salt is mainly located over the ocean and coastal areas, and it decreases latitudinally. The mass of MSA is lower than that of all

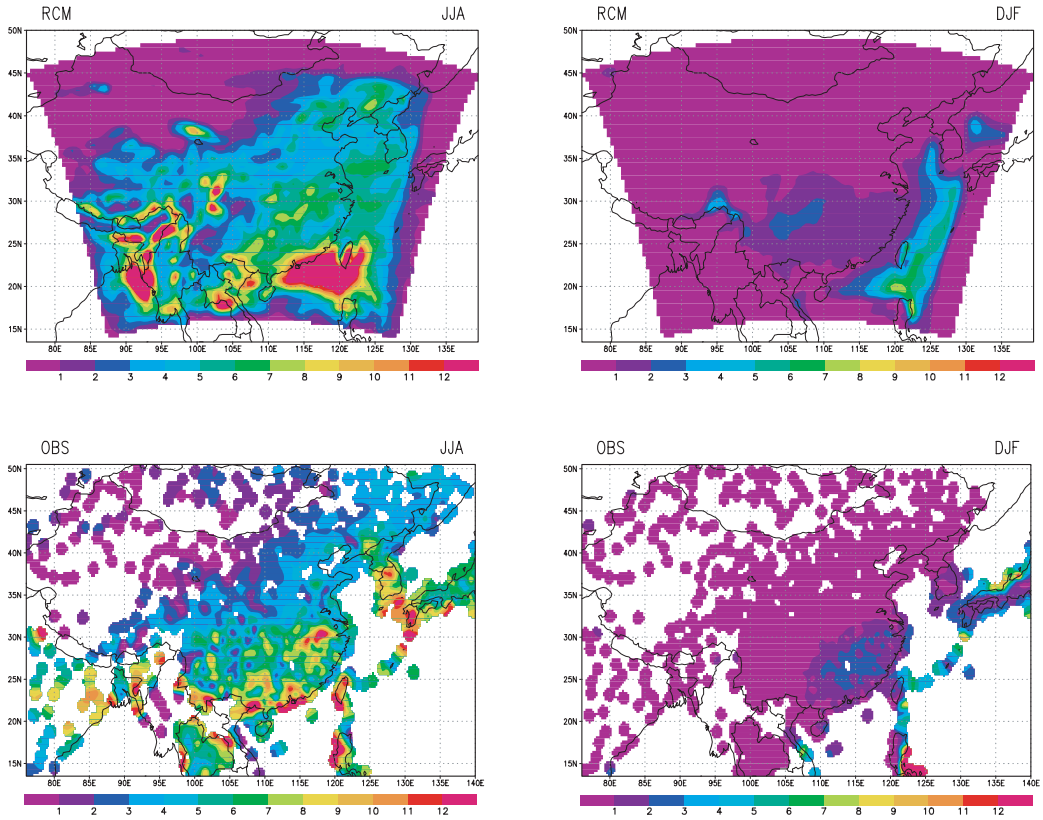

Fig. 3. Similar to Fig. 2 but for precipitation. Shading interval is 1 mm d^{-1}.

other aerosols and is mainly distributed over ocean and high-latitude areas. The mass of water in aerosol exhibits a pronounced maximum over the Sichuan Basin due to the combination of maximum water vapor, relative humidity and sulfate over the basin.

Table 3 summarizes the monthly and annual mean column mass of dry particles for the six chemical components and the total particle numbers in the four modes averaged over the China domain (20–45°N, 80–130°E). In the MIRAGE simulations sulfate is the primary aerosol over China and accounts for 60–70% in mass for both the accumulation and aitken modes. The mass of dry sulfate is greater in the warm season (June–October) for all modes. OC accounts for about 20% of the aerosol mass in the aitken mode, 30% in the accumulation mode and it is relatively high in the cold season. The seasonal cycle and spatial distribution of BC are closely tied to the patterns of OC, but the mass of BC is about one-tenth that of OC. The MSA, soil dust and sea salt only account for a very small fraction in the accumulation and aitken modes, while sulfate only accounts for less than 1% in the dust and sea-salt mode. These results are qualitatively consistent with limited observations of aerosol composition in some specific regions or sites in China (Su et al., 1989; He et al., 2001).

The particle number is maximum in the accumulation mode and accounts for over 60% of the total particle number. Second in abundance is the aitken mode, which accounts for close to 40% of the total particle number. The number of particles in the accumulation and aitken mode is two and five orders of magnitude higher than in the dust mode and sea salt mode, respectively. However, the total aerosol mass in the accumulation mode, which is close to that of the dust mode, is an order of magnitude higher than in the sea salt mode and three orders of magnitude higher than in the aitken mode, respectively, because of the different size and density of particles. It should be noted that the mass of water in aerosol is not

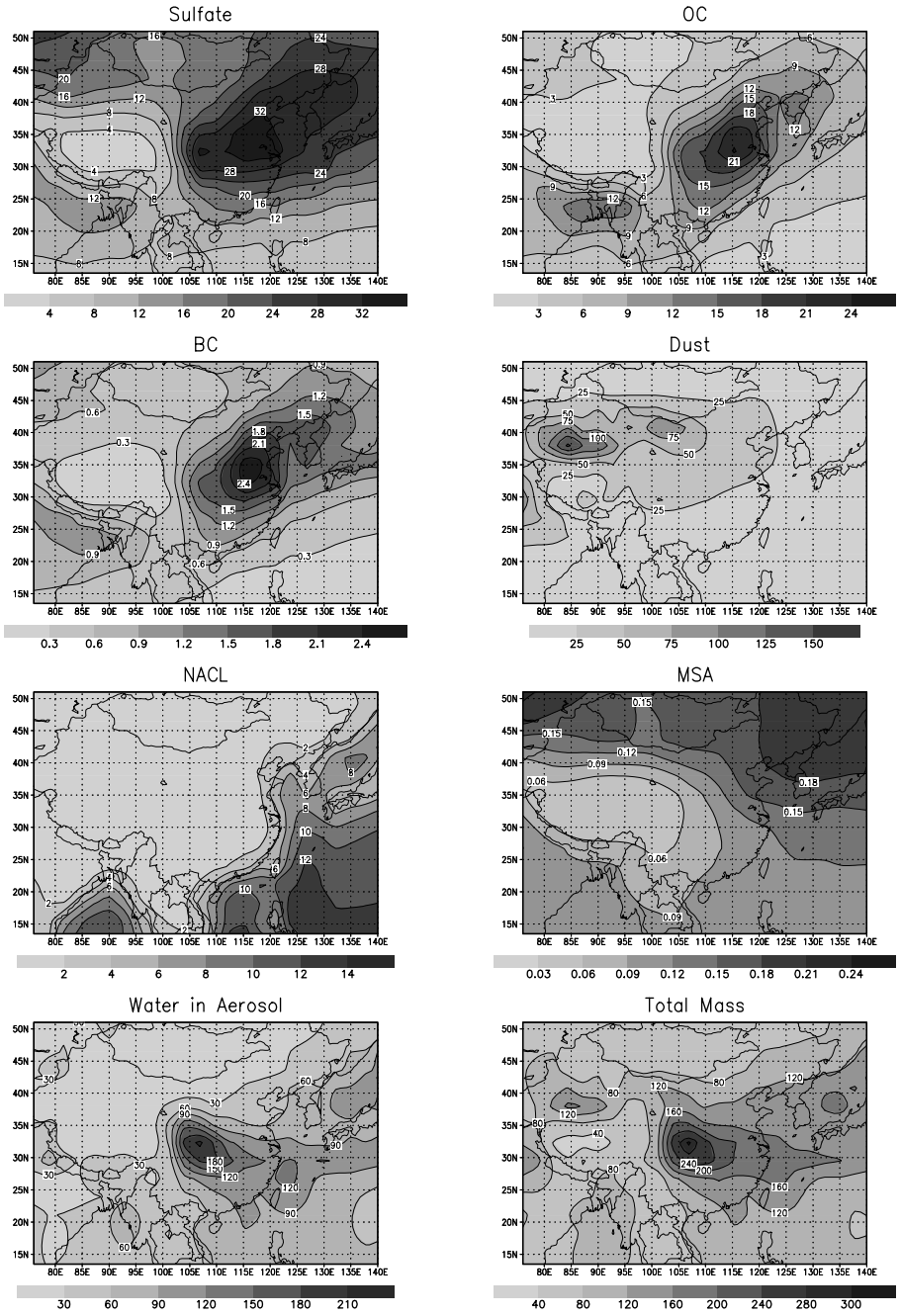

Fig. 4. Annual mean total column mass simulated by MIRAGE for sulfate, organic carbon (OC), black carbon (BC), dust, sea salt (NACL), MSA, water in aerosol and total sum. Units mg m^{-2}.

Table 3. *Monthly and annual mean column mass (g m^{-2}) for every chemical component and total particle number in four modes over the domain of China*

Mode		1	2	3	4	5	6	7	8	9	10	11	12	Annual	Percent
Accumulation	SO_4	1.4E-02[a]	1.6E-02	1.6E-02	1.5E-02	1.6E-02	1.7E-02	1.9E-02	1.9E-02	2.1E-02	1.7E-02	1.6E-02	1.4E-02	1.7E-2	63.1
	OC	8.4E-03	8.5E-03	8.8E-03	7.9E-03	7.9E-03	6.9E-03	6.5E-03	7.0E-03	7.9E-03	8.5E-03	9.8E-03	8.4E-03	8.0E-3	30.5
	BC	9.7E-04	1.0E-03	9.4E-04	7.8E-04	7.9E-04	7.9E-04	7.1E-04	7.1E-04	9.1E-04	8.7E-04	8.6E-04	7.8E-04	8.4E-4	3.20
	Dust	2.5E-04	3.5E-04	8.1E-04	1.2E-03	1.1E-03	9.3E-04	7.1E-04	5.7E-04	7.2E-04	3.1E-04	3.9E-04	3.8E-04	6.4E-4	2.45
	NaCl	1.3E-04	1.1E-04	9.6E-05	7.9E-05	7.3E-05	6.7E-05	8.3E-05	7.1E-05	5.1E-05	6.2E-05	8.4E-05	1.0E-04	8.4E-5	0.32
	MSA	2.0E-04	1.8E-04	1.4E-04	1.0E-04	8.4E-05	4.8E-05	4.9E-05	4.8E-05	5.2E-05	7.8E-05	9.5E-05	1.5E-04	1.0E-4	0.39
	Total	2.4E-02	2.6E-02	2.7E-02	2.5E-02	2.6E-02	2.5E-02	2.7E-02	2.7E-02	3.0E-02	2.7E-02	2.7E-02	2.4E-02	2.6E-2	100
Aitken	SO_4	5.7E-05	5.8E-05	5.0E-05	3.6E-05	3.2E-05	3.3E-05	1.0E-04	1.1E-04	3.8E-05	2.9E-05	4.0E-05	5.0E-05	5.3E-5	72.6
	OC	1.8E-05	1.8E-05	2.0E-05	1.9E-05	1.9E-05	1.5E-05	1.4E-05	1.5E-05	1.6E-05	1.8E-05	1.8E-05	1.9E-05	1.7E-5	23.7
	BC	1.9E-06	1.9E-06	1.8E-06	1.8E-06	1.7E-06	1.6E-06	1.5E-06	1.5E-06	1.7E-06	1.6E-06	1.6E-06	1.6E-06	1.7E-6	2.29
	MSA	2.5E-06	1.8E-06	1.1E-06	9.0E-07	7.6E-07	3.9E-07	3.4E-07	3.1E-07	3.3E-07	7.8E-07	1.3E-06	1.9E-06	1.0E-6	1.42
	Total	7.9E-05	8.0E-05	7.2E-05	5.8E-05	5.3E-05	5.0E-05	1.2E-04	1.3E-04	5.6E-05	4.9E-05	6.1E-05	7.3E-05	7.3E-5	100
Dust	SO_4	1.4E-04	1.7E-04	3.0E-04	3.5E-04	2.9E-04	3.0E-04	2.8E-04	2.7E-04	2.9E-04	1.7E-04	1.7E-04	1.4E-04	2.4E-4	0.80
	Dust	1.2E-02	1.5E-02	3.8E-02	5.2E-02	4.8E-02	4.0E-02	3.5E-02	2.7E-02	3.1E-02	1.4E-02	1.7E-02	1.7E-02	2.9E-2	99.2
	Total	1.2E-02	1.5E-02	3.9E-02	5.2E-02	4.9E-02	4.0E-02	3.6E-02	2.8E-02	3.1E-02	1.4E-02	1.7E-02	1.7E-02	2.9E-2	100
Sea salt	SO_4	2.5E-06	3.5E-06	3.7E-06	3.6E-06	3.1E-06	3.2E-06	6.4E-06	7.2E-06	6.5E-06	2.9E-06	3.4E-06	1.9E-06	4.0E-6	0.17
	NaCl	2.3E-03	2.4E-03	2.8E-03	3.0E-03	3.3E-03	1.7E-03	2.1E-03	2.1E-03	2.1E-03	2.2E-03	2.2E-03	2.1E-03	2.4E-3	99.8
	MSA	2.8E-07	2.6E-07	1.9E-07	1.4E-07	1.0E-07	7.3E-08	1.1E-07	1.2E-07	6.5E-08	4.6E-08	1.1E-07	1.6E-07	1.4E-7	0.03
	Total	2.3E-03	2.4E-03	2.8E-03	3.0E-03	3.3E-03	1.7E-03	2.1E-03	2.1E-03	2.1E-03	2.2E-03	2.2E-03	2.1E-03	2.4E-3	100
Number	Accumulation	6.2E+12	6.6E+12	6.8E+12	6.6E+12	6.8E+12	6.4E+12	6.5E+12	7.0E+12	7.1E+12	6.6E+12	6.7E+12	6.8E+12	6.7E12	62.5
	Aitken	5.8E+12	6.0E+12	5.0E+12	3.6E+12	3.0E+12	2.5E+12	3.1E+12	3.5E+12	2.8E+12	3.4E+12	4.0E+12	5.2E+12	4.0E12	37.3
	Dust mode	5.9E+09	8.2E+09	1.9E+10	2.8E+10	2.5E+10	2.1E+10	1.6E+10	1.3E+10	1.7E+10	6.9E+09	8.9E+09	8.7E+09	1.5E10	0.14
	Sea-salt	4.6E+07	4.0E+07	4.0E+07	3.9E+07	4.4E+07	3.8E+07	7.0E+07	6.9E+07	4.3E+07	3.5E+07	4.7E+07	4.4E+07	4.6E07	0.0004

[a] 1.4E-02 = 1.4×10^{-2} etc.

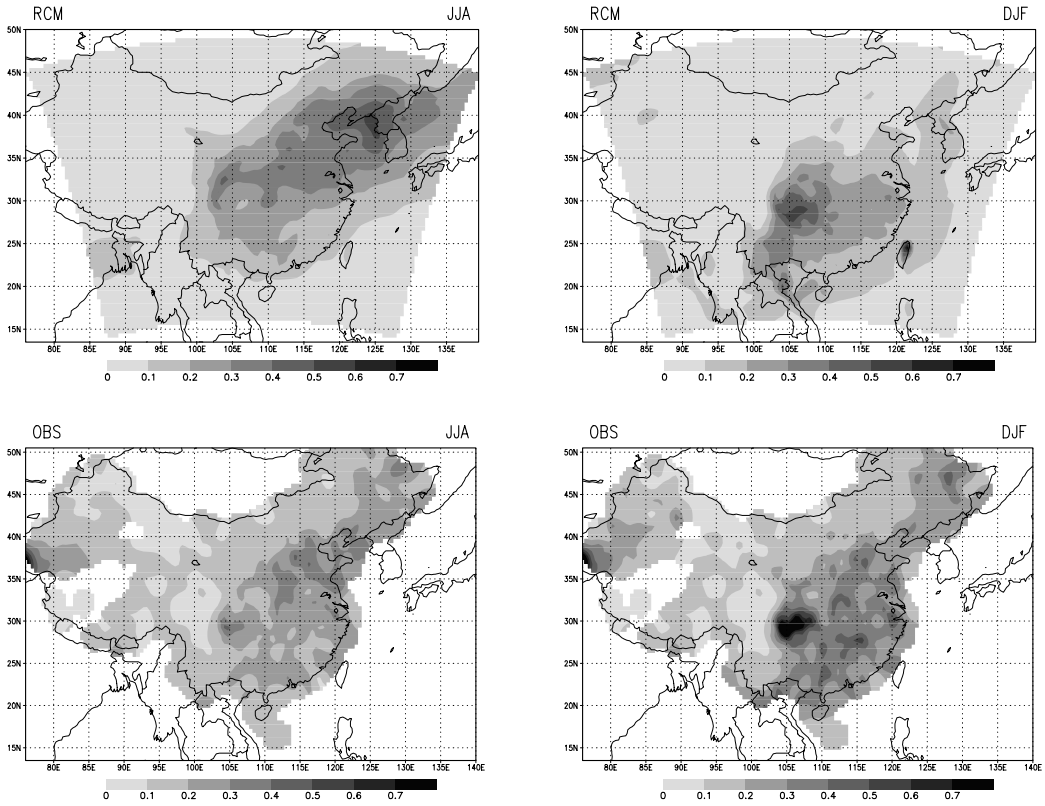

Fig. 5. Simulated (top) and observed (bottom) seasonal mean aerosol extinction coefficient (AEC) during JJA and DJF. Shading interval is 0.1 K m^{-1}.

included in Table 2. The actual mass of aerosol in the accumulation mode is possibly much larger than that in any other modes, since most of the highly soluble sulfate aerosol is in the accumulation mode.

3.2.2. Aerosol optical properties. Figure 5 shows the patterns of simulated and observed surface aerosol extinction coefficient (AEC) for JJA and DJF, respectively. Both observed and simulated AEC are averaged over the 5-yr simulation period. The model generally captures the observed aerosol spatial patterns in both JJA and DJF. In JJA, the region of maximum AEC extends from southwest to northeast China, with maxima over the Huabei region and the Bo Sea in Northeast China. The AEC is, however, generally underpredicted over south China and overpredicted over north China.

In DJF, the simulated AEC is largely lower than observed over east, south and north China. A reason for this bias is probably related to the different heights of the simulated and observed AEC. The simulated AEC corresponds to average values at the bottom atmospheric model layer, which has a thickness of about 50 m. Conversely, the observed AEC reflects the extinction properties at about 1.5 m height, since it is retrieved from surface visual range data. Therefore, the observed AEC possibly includes the effects of lifted dust near the surface, especially during the dry seasons (e.g. winter and fall). Another possible reason for the discrepancy between simulated and observed AEC is that a few measurements in special weather condition days (e.g. fog) are not excluded in the observed AEC, although data quality control methods are applied in retrieving the AEC.

The model correctly captures the most pronounced AEC maximum over the Sichuan Basin. This maximum is related to a maximum emission of aerosol precursors in this region (e.g. sulfur dioxide; Streets and Waldhoff, 2000). Furthermore, the abundant water vapor in the region facilitates the hygroscopic growth of soluble aerosol (e.g. sulfate). Local circulations

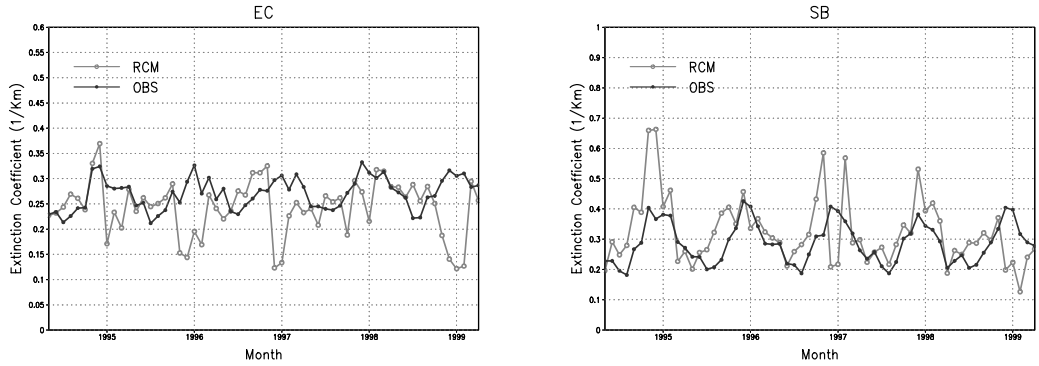

Fig. 6. Monthly mean aerosol extinction coefficient (AEC) based on observation and regional simulation. Units are K m^{-1}. (The time interval of the *x*-axis is month. For example, 1995 represents January 1995).

are likely another reason for the AEC maximum in the Sichuan Basin. Sheltered from large-scale winds, the basin is subject to persistent thermal inversions and stagnant conditions, which prevent efficient dispersion of locally produced aerosols. The AEC maximum over the Sichuan Basin was also found in previous observations (Li et al., 1995; Luo et al., 2000b; Qian and Giorgi, 2000) and modeling studies (Zhou et al., 1998; Chameides et al., 1999; Qian et al., 2001). In the simulation, the AEC amounts over west China in both JJA and DJF are underpredicted.

Figure 6 shows the variation of monthly mean AEC in the observations and simulation averaged over the Sichuan Basin (SB) and East China (EC) regions shown in Fig. 1. Over the EC region, the observed AEC is minimum in summer (around 0.22) and maximum in winter (around 0.33), a pattern consistent with the seasonal cycle of precipitation. In the summer, most aerosols are rapidly scavenged by the monsoon precipitation so that the atmospheric lifetime of aerosols is shorter than in the winter (Qian et al., 2001). The simulated AEC is generally close to the observed AEC except in winter, when the underestimation is up to 100% (see Fig. 5). The seasonal cycle of AEC is poorly simulated by the model over East China.

In the SB region, the AEC ranges from 0.2 to 0.4 in the observations with a more pronounced seasonal cycle than over East China. The model captures this seasonal cycle of the AEC well. The mean AEC for DJF from the observations is 0.374, which is very close to the simulated value (0.372). However, a stronger variability of AEC is found in the simulation during winter.

Simulated and observed annual mean aerosol optical depths (AOD) are shown in Fig. 7. The observed

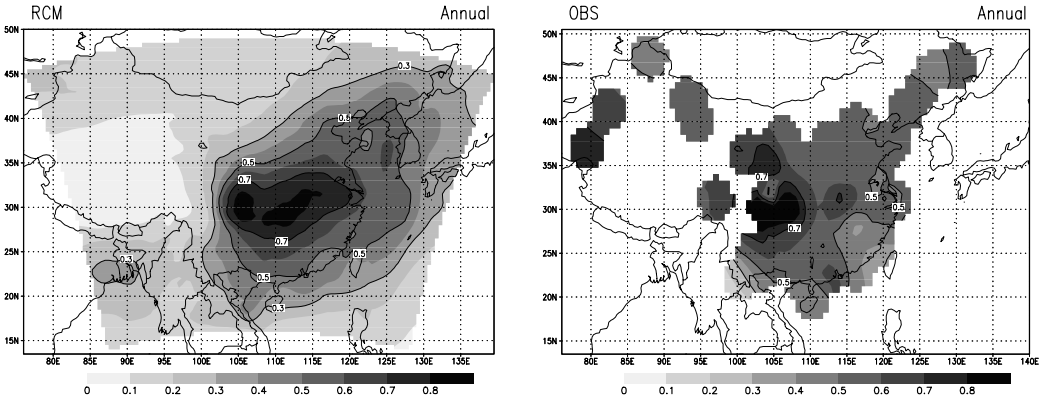

Fig. 7. Simulated and observed annual mean aerosol optical depth (AOD).

AOD at 0.55 μm is obtained from the AOD at 0.75 μm according to the procedure followed by Luo et al. (2000b; 2001) for 45 stations over China, which is based on the method provided by Chameides et al. (1999). The simulated annual AOD generally agrees well with observations both in magnitude and spatial distribution except for an overestimation over central–east China. The observations show that the AOD over most areas of China is greater than 0.5 except for a few coastal regions in south and East China. Maximum values of up to 0.8 are found over the Sichuan Basin. In Southwest China, the AOD gradually decreases from the Sichuan Basin to Laos. These features are reproduced well by the model. Note that the successfull simulation of the AOD is not inconsistent with the model underprediction of AEC, since the AEC refers to the surface layer, while the AOD accounts for the aerosol found in the entire atmospheric column. The successful simulation of the AOD provides a reliable foundation for estimating the radiative forcing and climatic effects of aerosols.

4. Climatic effects of aerosols

4.1. Simulated radiative forcing

The radiative forcing is defined as the change in the radiation balance of the surface–troposphere system imposed by external factors without any feedback; it is independently calculated in the DIR simulation based on two radiation calculations as described in section 2.2. Figure 8 shows the average aerosol direct radiative forcing (ADRF) for MAM (March–April–May), JJA, SON (September–October–November) and DJF. The ADRF is mostly negative because the incident solar radiation is reflected back to space by the aerosol particles (e.g. sulfate and OC) that dominate in this region. However, the ADRF varies spatially

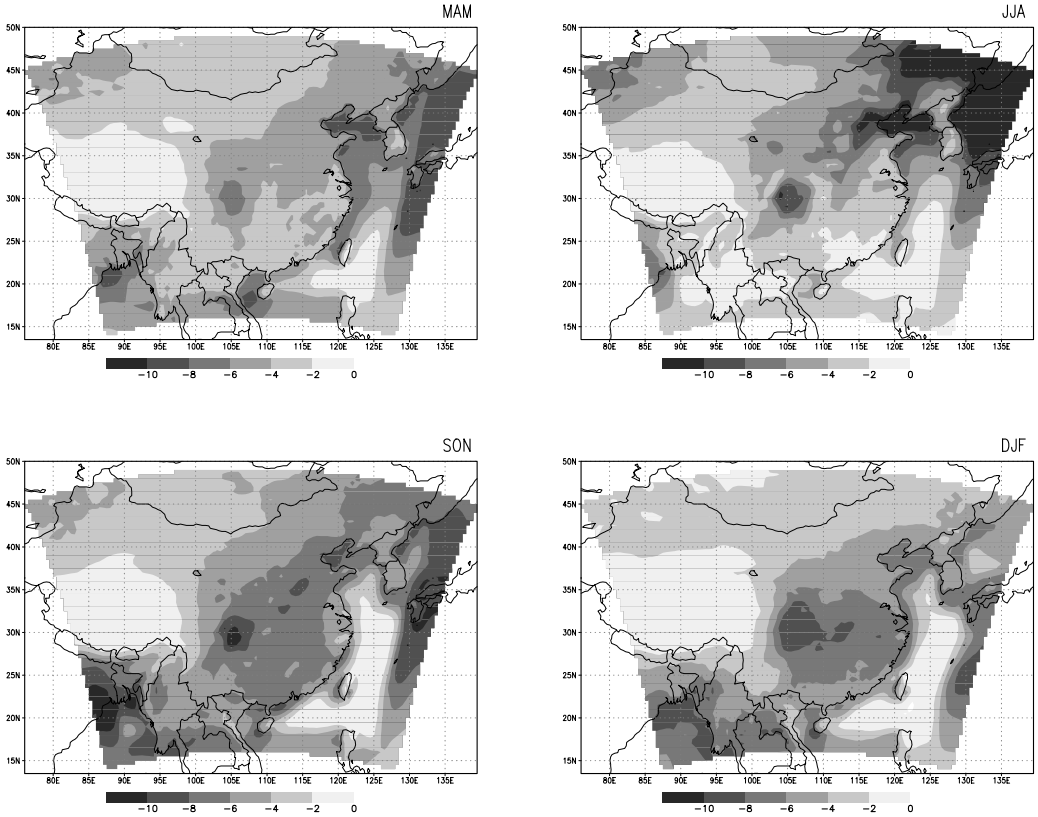

Fig. 8. Simulated aerosol direct radiative forcing (ADRF) for MAM (March–April–May), JJA (June–July–August, JJA), SON (September–October–November) and DJF (December–January–February). Shading interval is 2 W m^{-2}.

in the range –1 to –14 W m^{-2} in SON and JJA and −1 to –9 W m^{-2} in MAM and DJF. Regions of maximum negative ADRF generally correlate with regions of maximum AOD.

Maximum negative ADRF occurs in all seasons over the Sichuan Basin in response to the maximum aerosol loading there. Additional maxima are also found over East China in DJF and SON and Northeast China in MAM and JJA. However, we also find maximum negative ADRF over the Japan Sea, Northeast China and the Bay of Bengal where aerosol loadings are relatively low. The ADRF depends quite strongly on relative humidity (Kiehl and Rodhe, 1995), which is high over the oceans and coastal areas. The simulated spatial distribution of the ADRF in Fig. 8 generally agrees with previous simulations using general circulation models (Haywood et al., 1997; Kiehl et al., 2000; Ramaswamy, 2001) and regional climate models (G0203).

Table 4 shows the seasonal and annual mean change of radiative forcing and other climatic variables. The annual mean ADRF is –6.77 W m^{-2} averaged over SB and –5.11 W m^{-2} averaged over East China. Subregional averaged of ADRF in both SB and East China is usually 30–70% higher in SON and DJF than in MAM and JJA.

The annual mean ADRF calculated by G0203 was –4.32 and –2.52 W m^{-2} averaged over the Sichuan Basin and East China, respectively, when only anthropogenic sulfate and fossil fuel soot were considered under present day emissions. However, when doubling the sulfur emission, the concentration of sulfate and fossil fuel soot also nearly doubled, and the annual mean ADRF over the SB and East China reached −7.00 and –4.58 W m^{-2}, respectively. These values are close to those found in our simulations (−6.77 and –5.11 W m^{-2}), which indicates that the assumption of doubling sulfate concentrations in G0203 captured to a first-order approximation the radiative forcing of additional aerosols.

However, a further investigation of the seasonal variation of the ADRF reveals that in G0203 a negative ADRF maximum is found in the warm season and a minimum in the cold season, which is consistent with the seasonal cycle of anthropogenic sulfate burden in their model. Conversely, the ADRF is minimum in the warm season and maximum in the cold season in this study. The ADRF is 35–70% higher in DJF than that in JJA. One factor leading to this difference between G0203 and this work is the different seasonal cycle between sulfate and BC/OC (Table 3). Therefore, simply doubling the sulfur emission cannot describe the difference in seasonal cycle between sulfate and BC/OC burdens.

The spatial distribution of ADRF exhibits a more complex pattern than that in G0203, as more aerosols with different spatial distributions are in included in MIRAGE. The ADRF is larger over north China and some remote areas than that calculated by G0203, since dust, sea salt and MSA are not included in their study.

4.2. *Simulated temperature and precipitation response*

Figures 9a–9d show the simulated aerosol-induced surface air temperature change (the difference between DIR and CON) in the four seasons. Shading indicates that the difference is statistically significant at the 90% confidence level according to a two-tailed *t*-test. A general aerosol-induced cooling pattern is found over most areas of China in all seasons, especially east of 100°E, with a local maximum over the Sichuan Basin except for MAM. The cooling is in the range –0.6 to –1.2 °C in SON and DJF, –0.3 to –0.6 °C in MAM and

Table 4. *Seasonal and annual mean change of daily minimum temperature* (T_{min}, °*C*)*, daily maximum temperature* (T_{max}, °*C*)*, temperature* (T, °*C*)*, Prcp (Precipitation, mm d*$^{-1}$*) and aerosol direct radiative forcing* (*ADRF*, *Wm*$^{-2}$)

	SB					EC				
	MAM	JJA	SON	DJF	Annual	MAM	JJA	SON	DJF	Annual
$T_{\min}$	−0.55	−0.08	−0.31	−0.88	−0.46	−0.36	−0.01	−0.14	−0.73	−0.31
$T_{\max}$	−0.30	−0.97	−1.63	−1.33	−1.06	−0.49	−0.31	−1.27	−1.21	−0.82
T	−0.43	−0.53	−0.97	−1.11	−0.76	−0.42	−0.16	−0.70	−0.97	−0.56
Prcp	−0.21	0.04	−0.11	−0.21	−0.12	−0.17	−0.04	0.09	−0.09	−0.05
ADRF	−5.25	−5.97	−7.76	−8.10	−6.77	−4.05	−3.73	−6.42	−6.24	−5.11

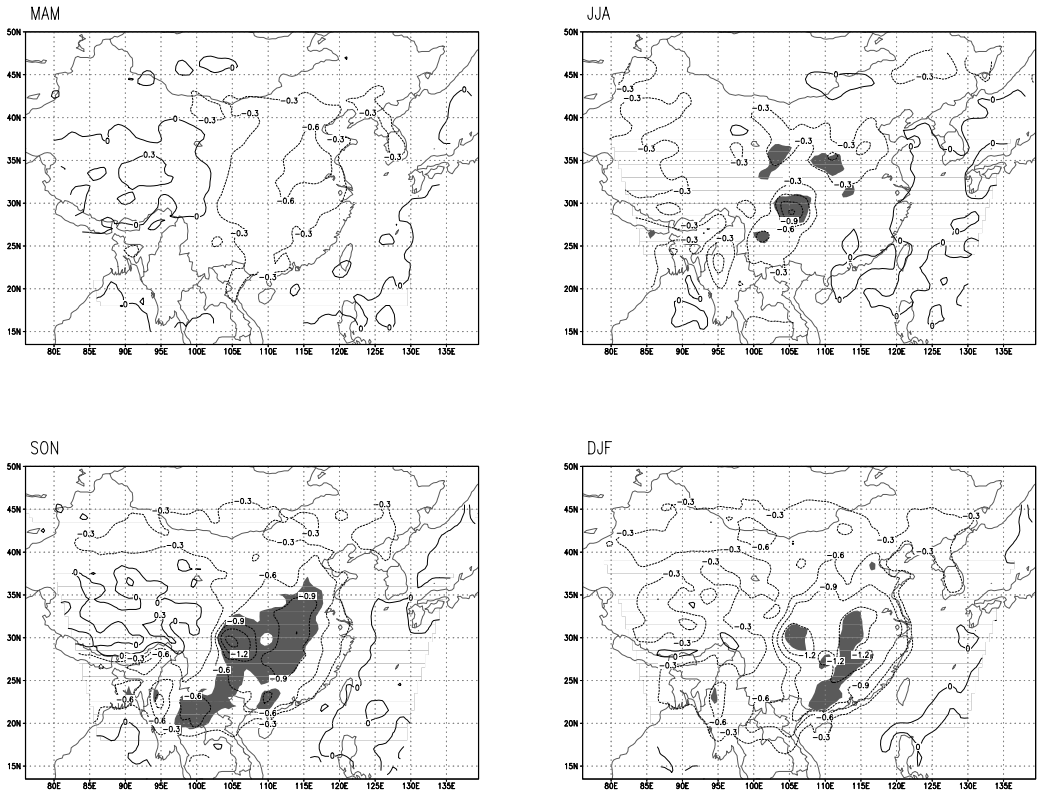

Fig. 9. Difference in average seasonal surface air temperature (°C) between the DIR and CON experiments. (a) MAM, (b) JJA, (c) SON, (d) DJF. Shading indicates areas in which the difference is statistically significant at the 90% confidence level.

0.0 to –0.9 °C in JJA over the Sichuan Basin and East China. One reason for the weaker aerosol radiative forcing and temperature response in MAM and JJA is the stronger cloud shading effect during the spring and summer monsoon seasons. The cooling in SON and DJF is approximately twice as large as that in MAM and JJA over the SB region, and 2–5 times higher in the East China (Table 4). These cooling signals are consistent with the negative radiative forcing over the corresponding regions. Because of the pronounced interannual variability and the small sample size (5 yr), no areas of statistically significant cooling are found in MAM. However, the aerosol-induced cooling is statistically significant over the Sichuan Basin and some areas of East and North China in SON, DJF and JJA.

Considering only direct effects of anthropogenic sulfate under present day sulfur emissions, the annual mean surface air temperature change calculated by G0203 was equal to −0.40 °C over the Sichuan Basin and −0.16 °C over East China. When the sulfur emission was doubled, the cooling reached −0.70 and −0.30 °C, respectively, which is still lower in magnitude than the cooling of −0.76 and −0.56 °C calculated in this work, especially over East China. Similarly to the case of ADRF, the primary difference between the doubled sulfur emission experiment in G0203 and this work is in the seasonal variation of the temperature change. For example, the aerosol-induced temperature change here reaches −0.97 °C over East China in DJF, compared to a corresponding value of −0.39 °C found by G0203. The difference of temperature change is small between the two studies in JJA. The seasonal variation of aerosol-induced temperature response is much stronger in our simulation than in that of G0203, since more aerosols with different seasonal cycles are included in our model. It is interesting that in our simulations both the ADRF and temperature response are maximum in DJF and minimum in JJA. In G0203, although the ADRF was somewhat greater in

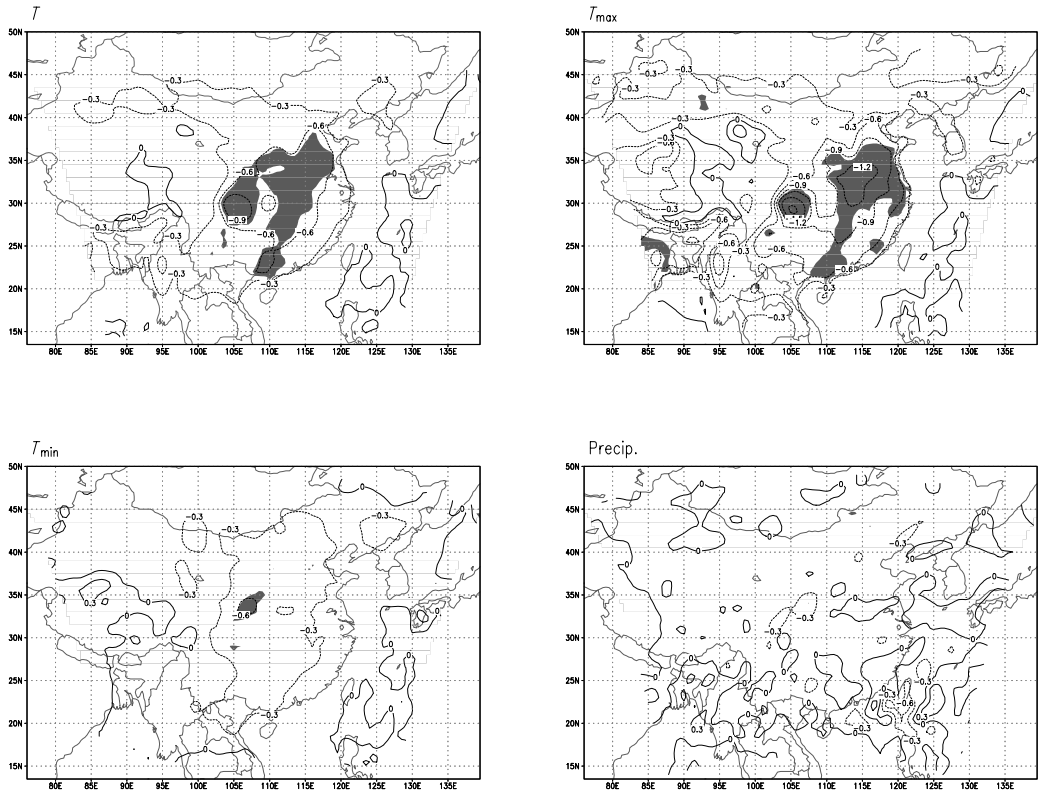

Fig. 10. Difference between DIR and CON for annual mean surface air temperature (T), daily maximum temperature ($T_{\max}$), daily minimum temperature ($T_{\min}$) and precipitation. Units are °C for temperature and mm d^{-1} for precipitation. Shading indicates areas in which the difference is statistically significant at the 90% confidence level.

JJA than in DJF, the temperature change was greater in DJF, as in our simulations.

Figures 10a–10d show the annual mean change of surface air temperature (T), daily maximum ($T_{\max}$) and minimum ($T_{\min}$) temperature, and precipitation due to the aerosol direct effects. The mean annual temperature decreases by 0.3 – 0.9 °C over most areas of China, with a local maximum over the Sichuan Basin. Cooling greater than 0.6 °C over the SB and the western part of East China is mostly statistically significant.

The decrease of $T_{\max}$ is in the range −0.6 to −1.2 °C over East China and up to −1.5 °C over the Sichuan Basin. Areas of statistically significant change in $T_{\max}$ are similar to those for the mean temperature (T). The effect of the aerosol forcing on $T_{\min}$ is much less evident compared to $T_{\max}$ and T, with smaller areas of statistically significant changes. Table 4 shows that the annual mean cooling for $T_{\max}$ is 40–46% more pronounced than for T and 130–160% than for $T_{\min}$.

This result is not surprising. The direct effect of scattering aerosols (e.g. sulfate and OC) is primarily to reflect the incident solar radiation back to space, while the effect of absorbing aerosols (e.g. BC) is to absorb the solar radiation. Both effects result in a reduction of the net solar radiation flux at the surface which in turn cause surface cooling (Chung et al., 2002; Menon et al., 2002). Generally, the effect of aerosols on the long-wave radiation is much less pronounced. Therefore, the aerosol forcing can be expected to affect primarily daytime maximum temperature (e.g. Harvey, 1995). The simulated aerosol-induced cooling in T is in fact mainly contributed by the daytime temperature change. The asymmetric response of daytime and night-time temperature to the aerosol direct effects suggests that not only mean temperature but also $T_{\max}$ (or daytime temperature) and $T_{\min}$ (or night-time temperature) should be investigated to identify the direct effects of aerosols on climate.

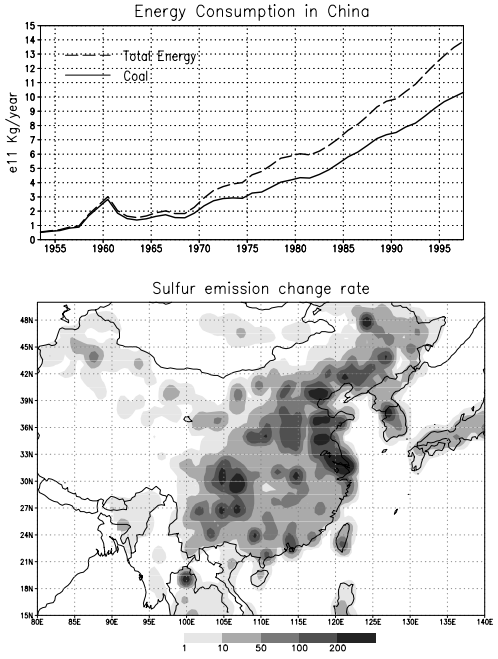

Fig. 11. (a) Yearly coal and total energy consumption (10^{11} kg yr^{-1}) in China from 1953 to 1997. (b) Spatial distribution of SO_2 emission yearly change rate (mg S m^{-2} yr^{-2}) during 1953 to 1997. The data are from Ren et al. (1997) and Streets and Waldhoff (2000).

Unlike Menon et al. (2002), an aerosol effect on precipitation is not evident in our simulation. Precipitation changes induced by aerosol are usually less than 5% and not statistically significant, as shown in Fig. 10d. G0203 found a general tendency of the aerosol-induced surface cooling to decrease precipitation, but also in their simulations when only the direct effects were included the precipitation response was small and mostly not statistically significant.

4.3. Aerosol-induced temperature signals in climate record

The results presented in section 4.2 suggest that atmospheric aerosols affect regional climate over China, even when only the direct effects are included. Continued and rapid increase of pollutant emission in China has resulted in a constant rise of aerosol concentration and optical thickness during the last decades (Qian and Giorgi, 2000; Luo et al., 2001). Figure 11a shows the temporal variation of the total energy and coal consumptions in China from 1953 to 1997. It can be seen that the energy consumption has increased significantly since 1953, when measurement data started to be available. Coal consumption in 1997 was about 20 times larger that in 1953, although the percentage of coal consumption within the total energy consumption has been decreasing in recent decades. The increase in energy consumption shown in Fig. 11a has led to a rapid increase in the emission of aerosol precursors (e.g. SO_2, Qian and Giorgi, 2000).

Figure 11b shows the spatial distribution of the yearly increase of SO_2 emission rate from 1953 to 1997. An increasing trend of sulfur emission rate is evident over the Sichuan Basin and East China, especially over some coastal areas of Northeast China. Because of the approximate linear relationship between anthropogenic aerosol concentration and pollutant emission rate (Penner, 2001; G0203), and the relatively short lifetime of sulfate (Qian et al., 2001), the spatial distribution and temporal trend in sulfate loading should be qualitatively similar to that shown in Figs. 11a and 11b. The spatial distribution and temporal trend of OC and BC should be, to some extent, similar to those of sulfate (see Fig. 4) since fossil fuel and biomass burning are the main sources of OC and BC. Therefore, has this remarkable change of aerosol loading in China left any signals in the observed climate record of the past decades?

Figures 12a–12d show the spatial distribution of the observed trend from 1953 to 1997 for the annual average surface air temperature (T), T_{max}, T_{min}, and precipitation based on the CRU 0.5 degree monthly observation land dataset. Shading indicates trends that are statistically significant at the 90% confidence level. For the most part, the East Asia region has undergone a statistically significant warming in the northern regions of the area (0.6–2.1 °C/45 yr) and over the Indochina peninsula (∼0.6 °C/45 yr). Comparing Figs. 12b and 12c, we find that the warming trend for T_{min} is much more evident than for T_{max}. Areas with statistically significant warming are much more widespread for T_{min} than for T_{max}. All these features, including the asymmetric trends of daily maximum and minimum temperature (Karl et al., 1993), are generally consistent with the warming trend observed in the northern hemisphere during the second half of the twentieth century, which has been mostly attributed to increasing concentrations of greenhouse gases (IPCC, 2001).

However, exceptions to the large-scale warming trend are found over the Sichuan Basin and extended areas of East China. In particular, cooling can be observed over the Sichuan Basin with magnitude in the

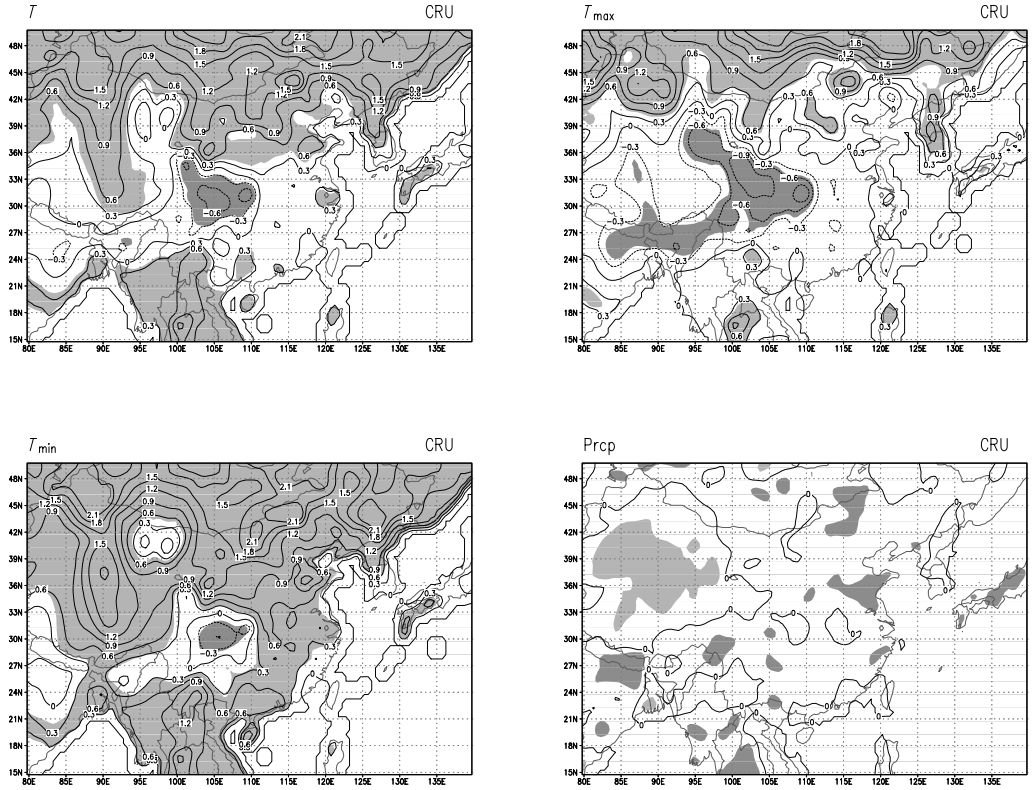

Fig. 12. The spatial distribution of observed trend (Units K 45 yr) from 1953 to 1997 for annual average surface air temperature (T), daily maximum temperature ($T_{\max}$), daily minimum temperature ($T_{\min}$) and precipitation (Prcp). CRU monthly data (New et al., 2000) are used in this figure and Fig. 13. Shading indicates areas in which the trend is statistically significant at the 90% confidence level.

range of -1 to -0.6 °C/45yr for T, -0.3 to -0.9 °C/45 yr for $T_{\max}$ and 0 to -0.3 °C/45 yr for $T_{\min}$. Therefore the observed cooling trend over this basin is mainly contributed by the decrease in $T_{\max}$. Over East China, the trend of T is less than -0.3 °C/45 yr. The trend of $T_{\max}$ is slightly negative (cooling), but that of $T_{\min}$ is positive (warming), with a magnitude in the range 0–0.6 °C/45 yr. Although we do not expect to find a one-to-one relationship between the simulated aerosol-induced and observed temperature signals, the observed cooling trends over these regions, as well as the fact that a decrease in $T_{\max}$ is the main contribution to this cooling, are consistent with the simulated effects of the aerosol forcing on temperature.

The trend in precipitation for 1953–1997 is generally small and not statistically significant (Fig. 12d). This is also consistent with the simulation of aerosol effects on precipitation, which is shown in Fig. 10d.

It is difficult clearly to identify and attribute the aerosol-induced signal in the long-term temperature record, because the observed trends may include the effects of natural climate variability (e.g. ENSO), increased greenhouse gas concentrations, and other human activities such as land use and land cover change. In an attempt to extract the aerosol signal, different modes of variability in the temperature record are decomposed using Principal Component Analysis. Figure 13 shows the time series of the first and second principal components (PC), and the corresponding spatial distributions of the empirical orthogonal function (EOF) based on summer mean temperature from 1953 to 1997. The time series of the first PC explains 26.9% of the total variance, and displays a strong interannual variability. The time series of the second PC explains about 15.1% of the total variance, and shows a significant decreasing trend, which is consistent with

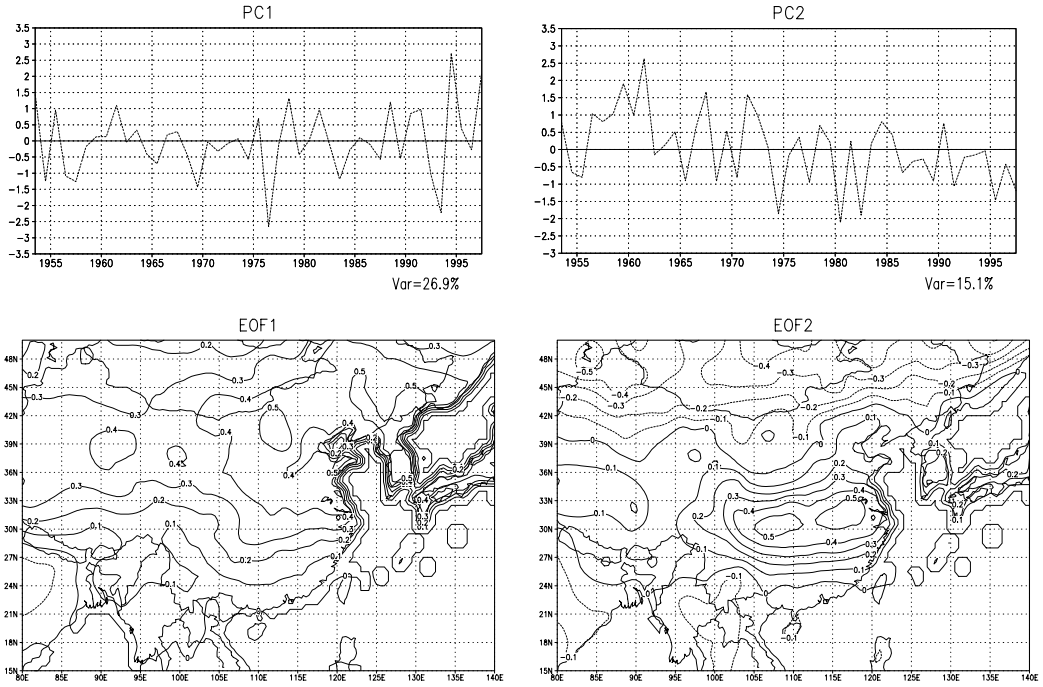

Fig. 13. Time series (top) of the principal component (PC) and the spatial distribution (bottom) of the first and second EOF (empirical orthogonal function) for summer mean temperature from 1953 to 1997.

the temporal cooling trend associated with the continued increase in aerosol loading over China. The spatial pattern of the second EOF shows a regional maximum over the Sichuan Basin and East China. This indicates that these regions, which are characterized in the model by the most pronounced aerosol cooling (Fig. 10), also contribute most significantly to the observed cooling trend found in the second PC (see Fig. 13). This suggests that the spatial pattern of the observed temperature trend in China is consistent with the temperature signal induced by the aerosol effect.

5. Conclusions and discussion

We have presented regional simulations of climate, aerosol physical and optical properties, direct radiative forcing and regional climatic effects of different natural and anthropogenic aerosols over China. We also analyzed the pollutant emissions and observed climatic data during the latter decades of last century in China. By comparing the simulations and the analysis of the observed record, we provide further evidence of possible relations between the observed climatic signals and aerosol trends over the region. Our primary conclusions can be summarized as follows:

1. The overall spatial distribution and seasonal patterns of temperature and precipitation are well simulated by the regional climate model, except for a cold bias of 2–3 °C for mean temperature (the same as for T_{max} and T_{min}) over most parts of China in JJA and a cold bias of 3–6 °C for T_{min} in DJF.

2. Sulfate and OC are the first and second primary aerosols in the accumulation and aitken modes. The seasonal cycle and spatial patterns of BC are tied to those of OC. Soil dust amounts are maximum in spring and are mainly distributed over Northwest China. The model generally captures the spatial patterns of AEC and AOD.

3. The radiative forcing of aerosol is in the range -1 to –14 W m^{-2} in SON and JJA and -1 to –9 W m^{-2} in MAM and DJF. It is characterized by substantial spatial variability at the regional scale. In particular, a strong maximum in negative radiative forcing corresponding to maximum aerosol optical depths is found in all seasons over the Sichuan Basin, where pollutant emission as well as relative humidity are high,

and stagnant atmospheric conditions inhibit pollutant dispersion.

4. The negative aerosol direct radiative forcing induces surface cooling, which is maximum in SON and DJF (−0.6 to −1.2 °C) and minimum in MAM (−0.3 to −0.6 °C) and JJA (0.0 to −0.9 °C) over the Sichuan Basin and East China due to more significant effects of cloud and precipitation in the summer and spring. The aerosol-induced cooling is mainly contributed by a decrease in maximum daytime temperature. The cooling is most pronounced and statistically significant over the Sichuan Basin. The effect of aerosol on precipitation is not statistically significant in our simulations.

5. The spatial patterns of temperature trends observed in the second half of the twentieth century, including the different trends in daily maximum and daily minimum temperature and an EOF analysis of the observed data, are consistent with the simulated aerosol-induced cooling over the Sichuan Basin and East China. Our results support the hypothesis that the observed temperature trends during the latter decades of the twentieth century, especially the cooling trends over the Sichuan Basin and some parts of East China, are at least partly related to the cooling induced by increasing atmospheric aerosol loadings. Aerosols that originate from the emission of anthropogenic pollutants have been increasing in concentration over China since the middle of the twentieth century.

6. G0203 captured to a first-order approximation the mean annual ADRF by doubling the current-day sulfur emissions. However, the seasonal cycle of the ADRF in their simulations was different from those we obtain because of the contribution of non-sulfate aerosols. The mean annual surface air temperature change calculated by G0203 is lower than that in this study, especially over East China. The seasonal variability of temperature effect of aerosol is stronger in our simulation than that in G0203, since more aerosols with different seasonalities are included in our model.

A number of limitations should be taken into account in evaluating our results. The primary one is that indirect aerosol effects are not accounted for. Giorgi et al. (2003), show that the indirect effects of sulfate are in the same direction as the direct effects and can therefore further amplify the aerosol-induced surface cooling. They also show that the indirect effects are especially important in the warm season over East Asia, when cloudiness and precipitation are maximum because of the onset and development of the monsoon. A second source of uncertainty is that our simulations do not account for regional-to-global feedbacks, i.e. they can only represent the local climatic impacts of the aerosol forcing. Third, any biases by the MIRAGE model in simulating aerosol distributions would affect the regional model. In particular, no interannual variation of aerosol concentration was considered in our experiments, since MIRAGE provided data only for one year. Uncertainties in estimating aerosol concentrations in MIRAGE are described in detail by Ghan et al., (2001a, b, c).

6. Acknowledgments

We thank Richard Easter for his constructive comments. This research is sponsored by the U.S. Department of Energy's (DOE) Office of Science Biological and Environmental Research under a bilateral agreement between the DOE and the China Meteorological Administration on climate change research and by the NASA Earth Science Enterprise under grant NAG5-9531. The research was performed at the Pacific Northwest National Laboratory (PNNL). PNNL is operated for the U.S. Department of Energy by Battelle Memorial Institute under contract DE-AC06-76RLO1830.

REFERENCES

Barrie, L. A., Yi, Y., Leaitch, W. R. and coauthors. 2001. A comparison of large-scale atmospheric sulphate aerosol models (COSAM): overview and highlights. *Tellus* **53B**, 615–645.

Benkovitz, C. M., Berkowitz, C. M., Easter, R. C., Nemesure, S., Wagener, R. and Schwartz, S. E. 1994. Sulfate over the North Atlantic and adjacent continental regions: Evaluation for October and November, 1986, using a three-dimensional model driven by observation-derived meteorology. *J. Geophys. Res.* **99**, 20 725–20 756.

Briegleb, B. P. 1992. Delta-eddington approximation for solar radiation in the NCAR community climate model. *J. Geophys. Res.* **97**, 7603–7612.

Chamedies, W. L., Yu, H. B., Liu S. C. and coauthors. 1999. A case study of the effects of atmospheric aerosols and regional haze on agriculture: An opportunity to enhance crop yields in China through emission controls? *Proc Natl. Acad. Sci.* **96**, 13 626–13 633.

Chen, F., Mitchell, K., Schaake, J., Xue, Y. K., Pan, H. L., Koren, V., Duan, Q. Y. and Betts, A. 1996. Modeling of land-surface evaporation by four schemes and

comparison with FIFE observations. *J. Geophys. Res.* **101**, 7251–7268.

Chung, E. C., Ramanathan, V. and Kiehl, J. K. 2002. Effects of the South Asia absorbing haze on the Northeast monsoon and surface–air heat exchange. *J. Climate* **15**, 2462–2476.

Ghan, S. J., Easter, R. C., Chapman, E., Abdul-Razzak, H., Zhang, Y., Leung, R., Laulainen, N., Saylor, R. and Zaveri, R. 2001a. A physically based estimate of radiative forcing by anthropogenic sulfate aerosol. *J Geophys. Res*. **106**, 5279–5293.

Ghan, S. J., Laulainen, N., Easter, R. C., Wagener, R., Nemesure, S., Chapman, E., Zhang, Y. and Leung, R. 2001b. Evaluation of aerosol direct radiative forcing in MIRAGE. *J. Geophys. Res.* **106**, 5295–5316.

Ghan, S.J., Easter, R. C., Hudson, J. and Breon, F. M. 2001c. Evaluation of aerosol indirect radiative forcing in MIRAGE. *J Geophys. Res.* **106**, 5317–5334.

Giorgi, F., Marinucci, M. R. and Bates, G. T. 1993a. Development of a second generation regional climate model (RegCM2). Part I: Boundary-layer and radiative transfer processes. *Mon. Wea. Rev.* **121**, 2794–2813.

Giorgi, F., Marinucci, M. R., Bates, G. T. and De Canio, G. 1993b. Development of a second generation regional climate model (RegCM2). Part II: Convective processes and assimilation of lateral boundary conditions. *Mon. Wea. Rev.* **121**, 2814–2832.

Giorgi, F., Bi, X. Q. and Qian, Y. 2002. Direct radiative forcing and regional climate effects of anthropogenic aerosols over East Asia: a regional coupled climate-chemistry/aerosol model study. *J. Geophys. Res*. **107**, 4439, 10.1029/2001JD001066.

Giorgi, F., Bi, X. Q. and Qian, Y. 2003. Indirect vs. direct effects of anthropogenic sulfate on the climate of East Asia as simulated with a regional coupled climate-chemistry/aerosol model. *Clim. Change*, **58**, 345–376.

Grell, G., Dudhia, J. and Stauffer, D. R. 1993. A description of the fifth generation Penn State/NCAR mesoscale model (MM5). *NCAR Tech. Note*, NCAR/TN-398+IA, Natl. Center for Atmos. Res., Boulder, CO, USA.

Hack, J. J., Boville, B. A., Briegleb, B. P., Kiehl, J. T., Rasch, P. J. and Williamson, D. L. 1993. Description of the NCAR Community Climate Model (CCM2). *NCAR Tech. Note* NCAR/TN-382+STR, Natl. Center for Atmos Res., Boulder. Co, USA, 108 pp.

Harvey, L. D. 1995. Warm days, hot nights. *Nature* **377**, 15–16.

Hayami, H. and Ichikawa, Y. 1995. Development of hybrid LRT model to estimate sulfur deposition in Japan. *Water, Air and Soil Pollution* **85**, 2015–2020.

Haywood, J. and Ramaswamy, V. 1998. Global sensitivity studies of the direct radiative forcing due to anthropogenic sulfate and black carbon aerosols. *J. Geophys. Res*. **103**, 6043–6058.

Haywood, J. M., Roberts, D. L., Slingo, A., Edwards, J. M. and Shine, K. P. 1997. General circulation model calculations of the direct radiative forcing by anthropogenic sulfate and fossil-fuel soot aerosol. *J. Climate* **10**, 1562–1577.

He K. B., Yang, F., Ma, Y., Zhang, Q., Yao, X., Chan, C. K., Cadle, S., Chan, T. and Mulawa, P. 2001. The characteristics of PM2.5 in Beijing, China. *Atmos. Environ.* **35**, 4959–4970.

Hong, S. Y. and Pan, H. L. 1996. Nonlocal boundary layer vertical diffusion in a medium-range forecast model. *Mon. Wea. Rev.* **124**, 2322–2339.

IPCC : Climate Change 2001: The Scientific Basis. Contribution of Working Group I to the Third Assessment Report of the Intergovernmental Panel on Climate Change (IPCC), (eds. J. T. Houghton, Y. Ding, D. J. Griggs, M. Nogure, P. J. van der Linden and X. Dai, Cambridge University Press, Cambridge, U.K.

Kaiser, D. P. and Qian, Y. 2002. Decreasing trends in sunshine duration over China for 1954 –1998: Indication of increased haze pollution? *Geophys. Res. Lett*. **29**, 2042, doi: 10.1029/2002GL016057.

Karl, T. R., Jones, P. D., Knight, R. W., Kukla, G., Plummer, N., Razuvayev, V., Gallo, K. P., Lindseay, J., Charlson, R. J. and Peterson, T. C. 1993. A new perspective on recent global warming: Asymmetric trends of daily maximum and minimum temperature. *Bull. Am. Meteorol Soc.* **74**, 1007–1023.

Kiehl, J. T. and Rodhe, H. 1995. Modeling geographic and seasonal forcing due to aerosols, In: *Aerosol forcing of climate*. (eds. R. J. Charlson and J. Heintzenberg), John Wiley, New York, 281–296.

Kiehl, J. T., Hack, J. J., Bonan, G. B., Boville, B. A., Briegleb, B. P., Williamson, D. L. and Rasch, P. J. 1996. Description of the NCAR Community Climate Model (CCM3). *NCAR Tech. Note*, NCAR/TN-420+STR, Nalt. Center for Atmos. Res.,Boulder, Co, USA,152 pp.

Kiehl, J. T., Schneider, T. L., Rasch, P. J., Barth, M. C. and Wong, J. 2000. Radiative forcing due to sulfate aerosols from simulations with the National Center for Atmospheric Research Community Climate Model, Version 3. *J. Geophys. Res.* **105**, 1441–1457.

Leung, L. R., Qian, Y. and Bian, X. 2003a. Hydroclimate of the western United States based on observation and regional climate simulation of 1981–2000. Part I: Seasonal statistics. *J. Climate*, **16**, 1892–1911.

Leung, L. R., Qian, Y., Bian, X. and Hunt, A. 2003b. Hydroclimate of the western United States based on observation and regional climate simulation of 1981–2000. Part II: Mesoscale ENSO anomalies. *J. Climate*, **16**, 1912–1928.

Li, X. W., Zhou, X. J. and Li, W. L. 1995. The cooling of Sichuan province in recent 40 years and its probable mechanism. *Acta Meteorol. Sin.* **9**, 57–68.

Liousse, C., Penner, J. E., Chuang, C., Walton, J. J., Edelman, H. and Cachier, H. 1996. A global three-dimensional model study of carbonaceous aerosols. *J. Geophys. Res.* **101**, 19 411–19 432.

Luecken D. J., Berkowitz, C. M. and Easter, R. C. 1991. Use of a three-dimensional clod-chemistry model to study the transatlantic transport of soluble sulfur species. *J. Geophys. Res.* **96**, 22 477–22 490.

Luo, C., John, J. C., Zhou, X., Lam, K. S., Wang, T. and Chameides, W. L., 2000a. A nonurban ozone air

pollution episode over eastern Asia: Observations and model simulations. *J. Geophys. Res*. **105**, 1889–1908.

Luo, Y. F., Lu, D. R. and He, Q. 2000b. Characteristics of atmospheric aerosol optical depth variation over China in recent 30 years. *Chinese Science Bulletin*. **45**, 1328–1334.

Luo, Y. F., Lu, D. R., Zhou, X. J., Li, W. L. and He, Q. 2001. Characteristics of the spatial distribution and yearly variation of aerosol optical depth over China in last 30 years. *J. Geophys. Res.* **106**, 14 051–14 513.

Menon, S., Hansen, J., Nazarenko, L. and Luo, Y. F. 2002. Climate effects of balck carbon aerosols in China and India. *Science* **297**, 2250–2253.

Middleton, W. E. K. 1954. *Vision through the atmosphere*. University of Toronto Press, Toronto, Canada, 250 pp.

New, M. G., Hulme, M. and Jones, P. D. 2000. Representing twentieth-century space time climate variability. Part II: Development of a 1961–1996 mean monthly terrestrial climatology. *J. Climate* **13**, 2217–2238.

Phadnis, M. J., Carmichael, G. R., Ichikawa, Y. and Hayami, H. 1998. Evaluation of long-range transport models for acidic deposition in East Asia. *J. App. Meteorol*. **37**, 1127–1142.

Penner, J. E. 2001. Aerosols, their direct and indirect effects. Chapter 5 in *Climate Change 2001, The Scientific Basis*, Contribution of Working Group I to the Third Assessment Report of the Intergovernmental Panel on Climate Change (eds. J. T. Houghton, Y. Ding, D. J.Griggs, M. Noguer, P. J. van der Linden and X. Dai), Cambridge University Press, Cambridge, U.K.

Qian, Y., Fu, C. B., Hu, R. M. and Wang, Z. F. 1996. Effects of industrial SO_2 emission on temperature variation in China and East Asia. *Clim. Environ. Res.* **2**, 143–149.

Qian, Y. and Giorgi, F. 1999. Interactive coupling of regional climate and sulfate aerosol models over eastern Asia. *J. Geophys. Res*. **104**, 6477–6499.

Qian, Y. and Giorgi, F. 2000. Regional climatic effects of anthropogenic aerosols? The case of Southwestern China. *Geophys. Res. Lett.* **27**, 3521–3524.

Qian, Y., Fu, C. B. and Wang, S. Y. 1999. Mineral dust and climate change. *Adv. Earth Sci.* **14**, 391–394 (in Chinese).

Qian, Y., Giorgi, F., Huang, Y., Chameides, W. L. and Luo, C. 2001. Regional simulation of anthropogenic sulfur over East Asia and its sensitivity to model parameters. *Tellus*. **53B**, 171–191.

Ramanathan, V., Crutzen, P. J., Kiehl, J. T. and Rosenfeld, D. 2001. Aerosols, climate, and the hydrological cycle. *Science* **292**, 2119–2124.

Ramaswamy, V. 2001. Radiative forcing of climate change. Chapter 6 *in Climate Change 2001, The Scientific Basis*, Contribution of Working Group I to the Third Assessment Report of the Intergovernmental Panel on Climate Change (eds. J. T. Houghton, Y. Ding, D. J. Griggs, M. Noguer, P. J. van der Linden and X. Dai), Cambridge University Press, Cambridge, U.K.

Reisner, J., Rasmusseb, R. J. and Bruintjes, R. T. 1998. Explicit forecasting of supercooled liquid water in winter storms using the MM5 mesoscale model. *Q. J. R. Meteorol. Soc.* **124B**, 1071–1107.

Ren, Z. H., Jiang, Z. Y., Yang, X. X. and Gao, Q. X. 1997. Research on the atmospheric transportaion, deposition and mutual influence of interprovince of acid materials over China. Acid rain and its control issue in China. China Center of Advanced Science and Technology, *World Laboratory Workshop Series*: **78**, 75–96.

Riches, M. R., Wang, W. C., Chen, P., Tao, S., Zhou, S. and Ding, Y. 2000. Recent Progress in the Joint Agreements on "Global and Regional Climate Change" Studies between the United States and the People's Republic of China. *Bull. Am. Meteorol. Soc*. **81**, 491–500.

Rodhe, H. 1999. Human impact on the atmospheric sulfur balance. *Tellus* **51A-B**, 110–122.

Streets, D. G. and Waldhoff, S. T. 2000. Present and future emissions of air pollutants in China: SO_2, NO_x, and CO. *Atmos. Environ.* **34**, 363–374.

Su, W. H., Zhang, Q. P., Song, W. Z., Luo, C. and Siu, Y. F. 1989. Problems of soot pollution and environmental-effects in northern China. *Aerosol Sci. Technol.* **10**, 231–235.

Troen, I. and Mahrt, L. 1986. A simple-model of the atmospheric boundary-layer-sensitivity to surface evaporation. *Boundary-Layer Meteorol*. **37**, 129–148.

Wang, W. X. 1997. The problems of environment acidification in China. *Acta Sci. Circum.* **17** (in Chinese).

Wei, F. S. 1995. Investigation of China SO_2 quality and emission standard. *China Environ. Monit.* **11**, 22–28 (in Chinese).

Xu, Q. 2001. Abrupt change of the mid-summer climate in central east China by the influence of atmospheric pollution. *Atmos. Environ.* **35**, 5029–5040.

Zhou, X. J., Li, W. L. and Luo, Y. F. 1998. Numerical simulation of the aerosol radiative forcing and regional climate effect over China. *Sci. Atmos. Sin.* **22**, 418–427.